Dalton Transactions

ROYAL SOCIETY OF CHEMISTRY

PAPER

View Article Online
View Journal | View Issue

Check for updates

Cite this: *Dalton Trans.*, 2025, **54**, 9778

$A_3Sc(PO_4)_2$ (A = Li, Na): rare earth cations effectively regulate phosphate structures for enhanced birefringence†

Hongheng Chen,‡[a] Xudong Leng,‡[a] Mei Hu,[a] Yibo Han,[a] Haiming Duan, [a] Qun Jing, *[a] Zhaohui Chen *[a] and Ming-Hsien Lee [b]

Received 14th March 2025,
Accepted 19th May 2025

DOI: 10.1039/d5dt00614g

rsc.li/dalton

Phosphates possessing a rich variety of structural types and intriguing properties are widely used in fields such as ionic conductors, phosphors, and nonlinear optical materials. In this paper, two novel rare earth phosphates, $A_3Sc(PO_4)_2$ (A = Li, Na), were successfully predicted using the artificial bee colony (ABC) algorithm along with *ab initio* total-energy calculations. The results of electronic structure and optical property calculations indicate that $A_3Sc(PO_4)_2$ (A = Li, Na) not only retains the advantage of the large bandgap (E_g) of phosphates but also ameliorates the defects of the smaller birefringence (Δn) of phosphates ($Li_3Sc(PO_4)_2$: E_g = 6.077 eV and Δn = 0.046@1064 nm; $Na_3Sc(PO_4)_2$: E_g = 5.085 eV and Δn = 0.058@1064 nm). The real-space atom-cutting (RSAC) results show that the birefringence of $A_3Sc(PO_4)_2$ (A = Li, Na) is mainly derived from the ScO_6 group. This study enriches the variety of rare earth phosphates and confirms that the introduction of rare earth cations is an effective strategy for obtaining phosphates with a balance of a large bandgap and suitable birefringence.

Introduction

Phosphates possess a rich variety of structural types, including PO_4 tetrahedra, P_2O_7 dimers, $(PO_3)_n$ chains, and super-anionic groups $[M(PO_4)_n]$ (M = Be^{2+}, B^{3+}, Al^{3+}, *etc.*).[1,2] This structural diversity endows phosphates with a range of intriguing properties, which are widely utilized in fields such as laser hosts, phosphors, ionic conductors, and birefringent materials.[3–9] It is well known that phosphates have relatively large bandgaps, for example, KH_2PO_4 (E_g = 7.04 eV),[10] $LiCs_2PO_4$ (E_g = 7.12 eV),[11] $LiRb_2PO_4$ (E_g = 7.29 eV),[12] $Ba_3P_3O_{10}X$ (X = Cl, Br) (E_g = 6.89 eV and >6.22 eV)[13] and $NH_4H_2PO_4$ (E_g = 6.74 eV),[14,15] among others. Unfortunately, similar to SO_4 and SiO_4 tetrahedra, PO_4 functional basic units (FBUs) with regular tetrahedra have small birefringence due to poor optical anisotropy. For example, $LiCs_2PO_4$ (Δn(cal) = 0.01@1064 nm),[11] $LiPbPO_4$ (Δn(cal) = 0.021@1064 nm),[16,17] $(H_3O)Ca_2Zn_{3.5}(PO_4)_4$ (Δn = 0.002@1064 nm),[18] and α-$LiZnPO_4$ (Δn = 0.005@1064 nm) all demonstrate small birefringence values.[19]

To overcome the drawback of the relatively small optical anisotropy coming from regular PO_4 tetrahedra, many strategies have been proposed.[20–23] In terms of anionic groups, the substitution of F^- and S^{2-} for O^{2-} of PO_4 tetrahedra has been employed to disrupt their high symmetry, resulting in FBUs like $[PO_3F]^{2-}$, $[PO_3S]^{3-}$, *etc.* This strategy could yield compounds with enhanced birefringence such as $(NH_4)_2PO_3F$ (Δn = 0.035@532 nm),[9] Na_2PO_3F (Δn = 0.036@532 nm),[24] Na_3PO_3S (Δn = 0.08@1064 nm),[25] and so on. On the cationic side, introduction of d^0/d^{10} cations or post-transition metal containing stereochemically active lone pairs was thought to be a good strategy to control the arrangement of PO_4 tetrahedra, as seen in compounds like $BaSn_2(PO_4)_2$ (Δn = 0.071@1064 nm)[26] and $LiHgPO_4$ (Δn = 0.068@1064 nm).[27] However, this strategy inevitably leads to a redshift of the bandgap. Therefore, it is of significant importance to seek strategies that can better balance the bandgap and birefringence in phosphates.

In recent years, rare-earth cations have become one of the important components in the design of new birefringent materials due to their unique electronic configurations and flexible coordination.[28–32] As shown in Fig. 1, rare-earth cations are capable of effectively balancing the bandgap and birefringence in phosphates. On one hand, cations such as Sc^{3+}, Y^{3+}, La^{3+}, and Lu^{3+} have closed-shell electron configurations, which can avoid d–d or f–f orbital transitions, thereby ensuring a large bandgap, as seen in compounds like $LiCs_2Y$

[a] *Xinjiang Key Laboratory of Solid State Physics and Devices, School of Physical Science and Technology, and Key Laboratory of Oil & Gas Fine Chemicals, Ministry of Education and Xinjiang Uyghur Autonomous Region, School of Chemical Engineering and Technology, Xinjiang University, Urumqi 830017, China. E-mail: qunjing@xju.edu.cn, chenzhaohui@xju.edu.cn*
[b] *Department of Physics, Tamkang University, New Taibei City 25137, China*

† Electronic supplementary information (ESI) available. See DOI: https://doi.org/10.1039/d5dt00614g

‡ These authors contributed equally to this work.

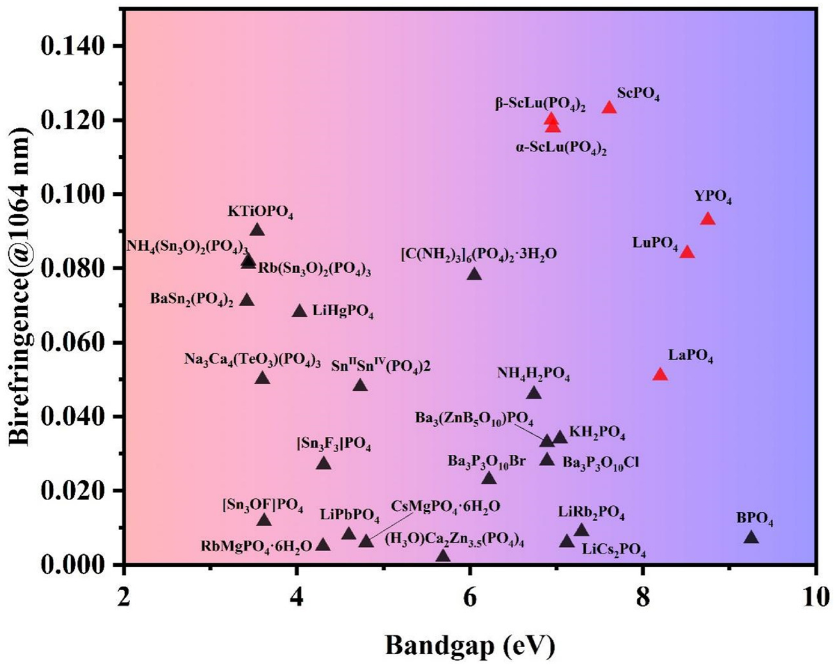

Fig. 1 The balance of the bandgap and birefringence of several orthophosphates.[10–18,26,27,35,36,62–71]

$(PO_4)_2$ (E_g = 6.20 eV)[33] and $YBa_3(PO_4)_3$ (E_g = 6.25 eV).[34] On the other hand, polyhedra formed from rare-earth cations can effectively control the arrangement of PO_4 tetrahedra, resulting in the enhancement of birefringence. For instance, Pan *et al.* have discovered a zipper-like arrangement in rare-earth phosphates that can effectively increase birefringence,[35] as in α-$ScLu(PO_4)_2$ (E_g(cal) = 6.94 eV; Δn(cal) = 0.120@1064 nm). Our group has also found enhanced birefringence in XPO_4 (X = Sc, Y, La, Lu); for example,$ScPO_4$ exhibits E_g(cal) = 7.61 eV and Δn(cal) = 0.123@1064 nm and YPO_4 exhibits E_g(cal) = 8.75 eV and Δn(cal) = 0.093@1064 nm,[36] in which the X–O bonds are perpendicular to the P–O bonds. The results mentioned above indicate that the strategy of introducing rare-earth cations is effective in balancing the bandgap and birefringence in phosphates. Consequently, rare-earth phosphates have become an important candidate system for ultraviolet (UV)/deep-ultraviolet (DUV) birefringent materials.

Hence, based on the inspiration from the reported DUV NLO material $A_3Sc(SO_4)_2$ (A = K, Rb, Cs),[37] this article successfully predicts a new type of rare-earth phosphate $A_3Sc(PO_4)_2$ (A = Li, Na) using the artificial bee colony (ABC) algorithm[38] combined with density functional theory (DFT) calculations.[39] Phonon spectrum analysis has proven its dynamic stability, and the electronic structure and optical properties of $A_3Sc(PO_4)_2$ (A = Li, Na) indicate that they both have excellent bandgaps and suitable birefringence ($Li_3Sc(PO_4)_2$: E_g = 6.077 eV, Δn = 0.046@1064 nm; $Na_3Sc(PO_4)_2$: E_g = 5.085 eV, Δn = 0.058@1064 nm). The electronic structural analysis and real-space atom-cutting (RSAC) results show that the birefringence of $A_3Sc(PO_4)_2$ (A = Li, Na) is mainly derived from the ScO_6 group. This research can help develop good nonlinear optical phosphates with a balance of a large bandgap and suitable birefringence.

Calculation details

Crystal structure screening

This paper utilizes the artificial bee colony (ABC) algorithm[38] implemented in the CALYPSO code[40,41] in conjunction with first-principles total energy calculations implemented in the VASP code[42,43] to screen and obtain the lowest energy structure of $A_3Sc(PO_4)_2$ (A = Li, Na). This method is capable of predicting the steady-state structures of given compounds under specified environmental conditions. During the screening process, the structures of $A_3Sc(PO_4)_2$ (A = Li, Na) were subjected to multiple searches with simulation cell sizes ranging from 1 to 2 formula units.

The crystal structure screening process is set as follows: (1) for each generation, the CALYPSO code[40,41] generates candidate structures, which are then locally optimized using the VASP code.[42,43] The number of candidate structures per generation is set to 50. (2) In the first generation, the code randomly generates different cells, and atoms are filled into random positions using symmetry constraints to produce the first generation of structures. In the subsequent generations, 60% of the structures are generated based on the characteristics of the previous generation, while the remaining 40% of the structures are generated using the same method as the first generation. (3) After 50 generations of structural evolution, the stable structure of $A_3Sc(PO_4)_2$ (A = Li, Na) is ultimately obtained.

The dynamic stability of $A_3Sc(PO_4)_2$ (A = Li, Na) is further evaluated using the phonon spectrum obtained with the VASP code.[42,43] The geometries obtained using the CALYPSO code are relaxed using the conjugate gradient (CG) method[44,45] until the force is less than 0.02 eV $Å^{-1}$. During the geometry relaxation, the cutoff energy is set to 400 eV, with the Perdew–Burke–Ernzerhof (PBE)[46] functional under the generalized gradient approximation (GGA)[47] and the norm-conserving pseudopotentials (NCP)[48]. To harmonize calculation standards, the Monkhorst–Pack *k*-point grids[49] in the computational codes in this paper (including VASP,[42,43] CASTEP,[50] and PWmat[51,52]) are all set to an accuracy of 0.04 $Å^{-1}$. The phonon spectrum is then obtained using the perturbation method.

Electronic structure and optical properties

The electronic structure and optical properties of $A_3Sc(PO_4)_2$ (A = Li, Na) were further calculated using CASTEP software.[50] The structure of $A_3Sc(PO_4)_2$ (A = Li, Na) was obtained through the crystal structure screening method described above. During the computation, the exchange–correlation functional is chosen as the GGA–PBE functional,[46,47] and the pseudopotential was selected as the NCP.[48] The valence electron configurations were as follows: Li: $2s^1$, Na: $2s^22p^63s^1$, Sc: $3s^23p^63d^14s^2$, P: $3s^23p^3$, and O: $2s^22p^4$. The cutoff energy is set to 830 eV, and the Monkhorst–Pack *k*-point grids of those compounds were set as 5 × 5 × 4 ($Li_3Sc(PO_4)_2$-$C2/m$) and 5 × 5 × 5 ($Na_3Sc(PO_4)_2$-$R\bar{3}m$). To achieve convergence in geometry optimization, the total energy convergence criterion was set to 5.0×10^{-6} eV, and the convergence criteria for maximum atomic force, maximum stress, and maximum displacement were set to 0.01 eV $Å^{-1}$, 0.02 GPa, and 5.0×10^{-4} Å, respectively. All other calculation parameters and convergence criteria were set to the default values of the CASTEP[50] software package.

Due to the discontinuity of the exchange–correlation functional, the bandgap obtained using GGA–PBE[46,47] is often underestimated.[53] Therefore, in this paper, the hybrid functional (HSE06)[54,55] band structures of the materials were also calculated using the PWmat code.[51,52] During the calculation process, the CG method is used for structural optimization and the cutoff energy is set to 70 Ry. The Monkhorst–Pack *k*-point grids of the compounds were set as 5 × 5 × 4 ($Li_3Sc(PO_4)_2$-$C2/m$) and 5 × 5 × 5 ($Na_3Sc(PO_4)_2$-$R\bar{3}m$). The convergence criterion for atomic forces was set to 0.01 eV $Å^{-1}$, and the convergence criterion for lattice stress was set to less than 0.01 eV per N atom. The other computational parameters and convergence criteria retained the default values of the PWmat code.[51,52]

The refractive index of $A_3Sc(PO_4)_2$ (A = Li, Na) is obtained through CASTEP calculations, and then the birefringence is determined. During the calculation process, the scissors operator is set to 1.421 eV ($Li_3Sc(PO_4)_2$-$C2/m$) and 1.726 eV ($Na_3Sc(PO_4)_2$-$R\bar{3}m$), respectively. The contribution of each group in the material to its optical properties was analyzed using the real-space atom-cutting (RSAC) method.[56] The underlying principles are explained in ref. 56 and the ESI.† According to the principle that the cutting spheres touch but do not overlap, the atomic cutting radii were set as follows: Li: 0.68 Å, Na: 1.095 Å, Sc: 1.82 Å, P: 1.06 Å, and O: 1.10 Å.

Results and discussion

$A_3Sc(PO_4)_2$ (A = Li, Na) crystal structure

Using the method described above, the most stable and metastable candidates of $A_3Sc(PO_4)_2$ (A = Li, Na) were obtained. Interestingly, during the structural screening process, approximately 6740 candidates of $Li_3Sc(PO_4)_2$ were identified. These candidates were distributed across only 79 space groups (as shown in Fig. 2a), of which 55.9% belong to non-centrosymmetric (NCS) space groups. For $Na_3Sc(PO_4)_2$, 3385 candidate structures were obtained, which are primarily distributed across 62 space groups (shown in Fig. 2c). Among these, candidate structures belonging to the NCS space groups account for 55% of the total number of structures. According to the total energy of these candidates, about 15 lower-energy structures of $A_3Sc(PO_4)_2$ (A = Li, Na) were selected (shown in Fig. 2b and d).

The formation energy calculations for the structures with lower energy are shown in Table S1 of the ESI.† According to Fig. 2b, the most stable structure for $Li_3Sc(PO_4)_2$ is the $C2/m$ space group. For $Na_3Sc(PO_4)_2$, the most stable structure is the $R\bar{3}m$ space group. The results show that the formation energies of $A_3Sc(PO_4)_2$ (A = Li, Na) are all less than zero, proving that both structures have the possibility of experimental synthesis. The dynamic stability of these candidates is further evaluated using the phonon spectrum. The obtained phonon spectra of the candidate structures of $Li_3Sc(PO_4)_2$-$C2/m$ and $Na_3Sc(PO_4)_2$-$R\bar{3}m$ are given in Fig. 3. As shown in Fig. 3, all these candidate structures are dynamically stable because no imaginary frequencies are found in their phonon spectra. Hereafter, the authors would pay more attention to the electronic structures and optical properties of these candidate structures.

The crystal geometries of these candidate structures of $A_3Sc(PO_4)_2$ (A = Li, Na) are illustrated in Fig. 4. For $A_3Sc(PO_4)_2$ (A = Li, Na), as shown in Fig. 4, a Li (Na) atom is connected to six surrounding O atoms to form a $Li(Na)O_6$ polyhedron, which serves as a filler module in the structure. A Sc atom is connected to six surrounding O atoms to form a ScO_6 octahedron, and a P atom is connected to four surrounding O atoms to form a PO_4 tetrahedron. The ScO_6 octahedron and the PO_4 tetrahedron are functional modules in the structure. Baur's method[57] implemented in the VESTA code[58] was employed to calculate the distortion indices of various groups in $A_3Sc(PO_4)_2$ (A = Li, Na), and the results are presented in Table S2.† The formula for calculating the distortion index is as follows:

$$D = \frac{1}{n}\sum_{i=1}^{n}\frac{|l_i - l_m|}{l_m}$$

Here, D is the distortion index, with a larger value indicating more severe distortion; n is the total number of bonds in the polyhedron; l_i is the length of the i-th bond; and l_m is the

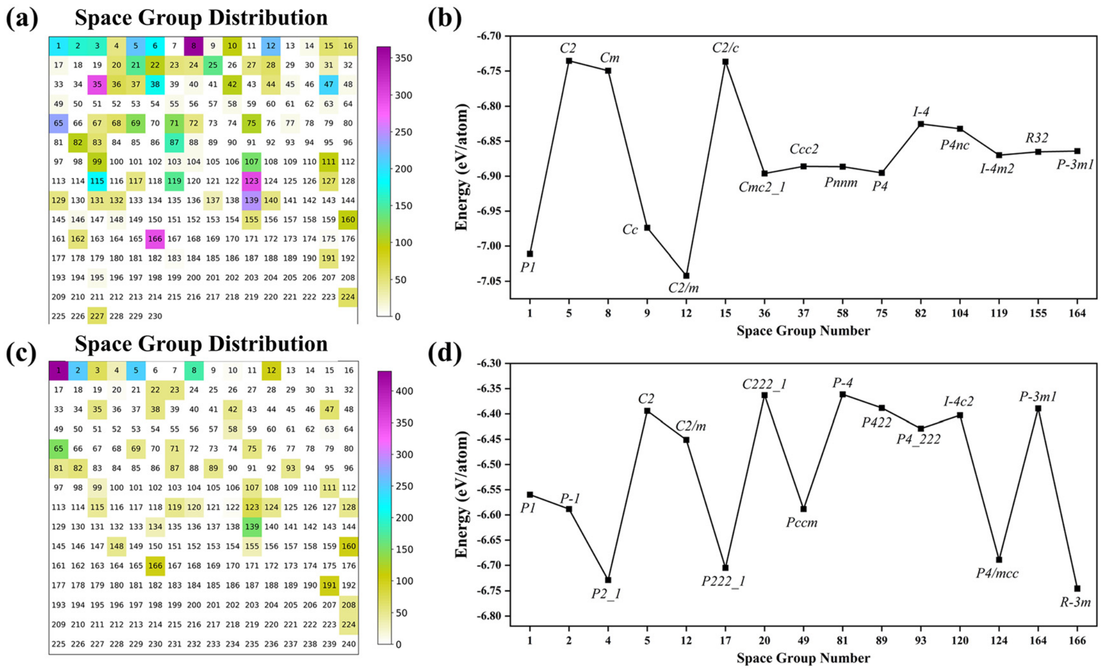

Fig. 2 (a) and (c) The distribution of space groups in $A_3Sc(PO_4)_2$ (A = Li, Na) structures; the color scale in the figure represents the number of structures crystallizing in the space group, with colors closer to purple indicating a higher number of structures; (b) and (d) the 15 lower-energy structures of $A_3Sc(PO_4)_2$ (A = Li, Na).

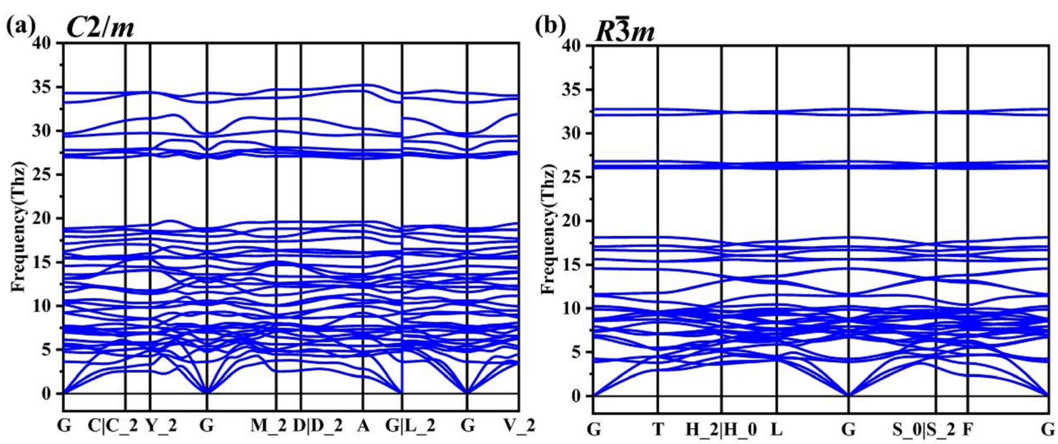

Fig. 3 The phonon spectra of the candidate structures of $Li_3Sc(PO_4)_2$ (a) and $Na_3Sc(PO_4)_2$ (b).

average bond length of the n bonds. From the data in Table S2,† the functional module ScO_6 octahedron does not exhibit distortion and has a regular octahedral structure; the PO_4 tetrahedron has a very small distortion, with a value of 0.016. Six PO_4 tetrahedra are arranged axially symmetrically around the Sc atom to form a "pinwheel" structure; similar "pinwheel" structures have also been found in other rare earth phosphates, such as $K_3RE(PO_4)_2$ (RE = Sc, Y, La, Lu) and so on.[59–61] The Li (Na) atoms fill the structural interstices and serve to balance the charge. In the three candidate structures of $A_3Sc(PO_4)_2$ (A = Li, Na), the PO_4 tetrahedra and ScO_6 octahedra are connected through corner-sharing to form a two-dimensional layered structure.

It is noteworthy that in $Li_3Sc(PO_4)_2$-$C2/m$ and $Na_3Sc(PO_4)_2$-$R\bar{3}m$, the PO_4 tetrahedra exhibit an interleaved distribution, which is a zipper-like arrangement (as shown in Fig. 4(b) and (d)). In their study of rare-earth phosphates, Pan and colleagues[35] found that the zipper-like arrangement of PO_4 groups, regulated by rare-earth cations, is very helpful in improving the small birefringence of phosphates. Therefore, even with a small distortion index in the functional modules, the $A_3Sc(PO_4)_2$ (A = Li, Na) obtained in this paper can still

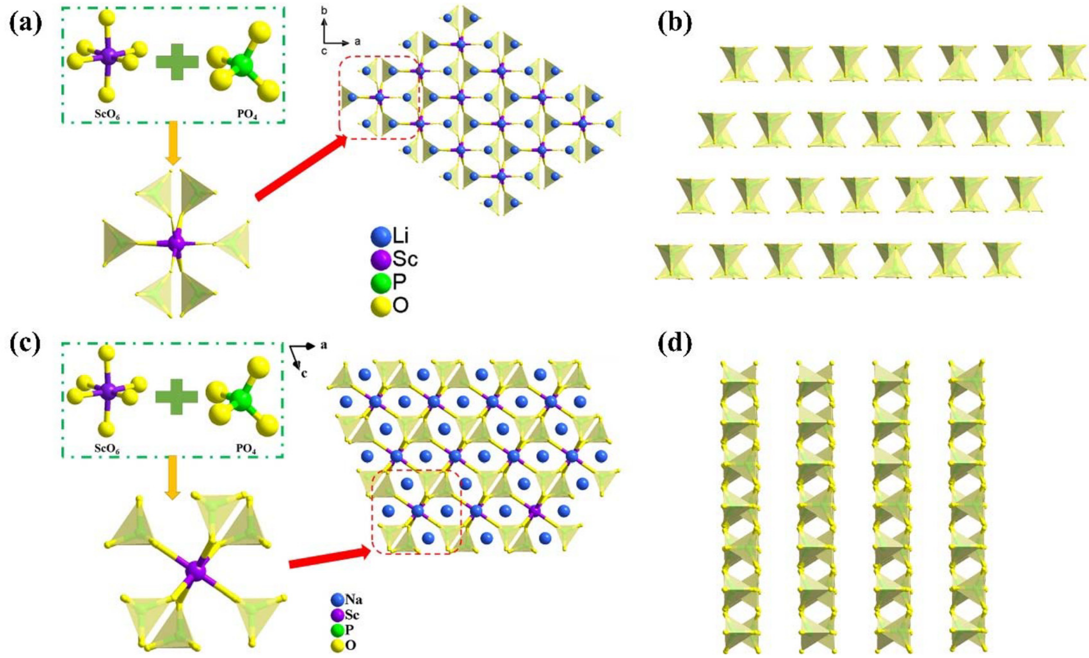

Fig. 4 (a) and (b) The crystal structure of $Li_3Sc(PO_4)_2$-$C2/m$ and the arrangement of the PO_4 groups; (c) and (d) the crystal structure of $Na_3Sc(PO_4)_2$-$R\bar{3}m$ and the arrangement of the PO_4 groups.

achieve excellent birefringence (further details are discussed below).

Electronic structure of $A_3Sc(PO_4)_2$ (A = Li, Na)

The band structures are also obtained (as shown in Fig. 5). Fig. 5a and c show the obtained GGA–PBE band structures of $Li_3Sc(PO_4)_2$-$C2/m$ and $Na_3Sc(PO_4)_2$-$R\bar{3}m$. For $Li_3Sc(PO_4)_2$-$C2/m$, the maximum of the valence band (VBM) is located at the high-symmetry point G, and the minimum of the conduction band (CBM) is located at the high-symmetry point M, with an indirect bandgap value of 4.656 eV. For $Na_3Sc(PO_4)_2$-$R\bar{3}m$, the VBM is located at the high-symmetry point F, and the CBM is located at the high-symmetry point G, with an indirect bandgap value of 3.359 eV. Considering the discontinuity of the GGA–PBE exchange–correlation functional, which inevitably leads to an underestimation of the bandgap, we calculated the HSE06 bandgaps for title compounds using the PWmat code.[51,52] As shown in Fig. 5b and d, the HSE06 band structure results indicate that both compounds remain indirect bandgap semiconductors, whose HSE06 bandgaps are 6.077 eV ($Li_3Sc(PO_4)_2$-$C2/m$) and 5.085 eV ($Na_3Sc(PO_4)_2$-$R\bar{3}m$), implying that these compounds could be used as UV optical materials. Notably, although the introduction of d^0/d^{10} cations or cations with stereochemically active lone-pair distribution can enhance birefringence, this strategy could lead to the red-shift of bandgaps, for example: $KTiOPO_4$ (E_g = 3.54 eV),[62] $LiPbPO_4$ (E_g = 4.60 eV),[16,17] $LiHgPO_4$ (E_g = 4.03 eV),[27] $K_2TeP_2O_8$ (E_g = 4.59 eV),[63] $CsMgPO_4{\cdot}6H_2O$ (E_g = 4.80 eV),[64] and so on. In contrast, the introduction of rare-earth cations effectively maintains the advantage of the large bandgap in phosphates, with their working wavelength region close to the DUV region.

We obtained the PDOS (projected density of states) of $A_3Sc(PO_4)_2$ (A = Li, Na), as shown in Fig. 6. For $Li_3Sc(PO_4)_2$, the top of the valence band (VB) is primarily contributed by O-p orbitals and a small number of Li-s, P-p, and Sc-d orbitals. The bottom of the conduction band (CB) is mainly contributed by Sc-d orbitals and a small number of Li-s, O-p, and P-p orbitals. Near the Fermi surface, there are Sc–O and P–O hybridized orbitals, which exhibit the characteristics of Sc–O and P–O covalent bonds. For $Na_3Sc(PO_4)_2$, its PDOS is similar to that of $Li_3Sc(PO_4)_2$, as shown in Fig. 6b. The PDOS results indicate that the large bandgap is primarily determined by the O-p orbitals at the top of the valence band (VB) and the Sc-d orbitals at the bottom of the conduction band (CB). It is noteworthy that the presence of Sc–O covalent bonds near the Fermi surface indicates that the ScO_6 groups are the determining factor for the optical effects in $A_3Sc(PO_4)_2$ (A = Li, Na).

Birefringence and its origin in $A_3Sc(PO_4)_2$ (A = Li, Na)

Table 1 and Fig. 7 list the refractive indices and birefringence values of $A_3Sc(PO_4)_2$ (A = Li, Na) calculated at wavelengths of 532 nm and 1064 nm. As shown in Table 1 and Fig. 7, the $Li_3Sc(PO_4)_2$-$C2/m$ crystal belongs to the centrosymmetric space group $C2/m$ and is a biaxial crystal. The calculated refractive indices are 1.807(n_x), 1.801(n_y), and 1.755(n_z)@532 nm, and 1.773(n_x), 1.764(n_y), and 1.726(n_z)@1064 nm, respectively, distributed according to the rule $n_x > n_y > n_z$. The calculated birefringence values are 0.052@532 nm and 0.046@1064 nm. $Na_3Sc(PO_4)_2$-$R\bar{3}m$ crystallizes in the centrosymmetric space

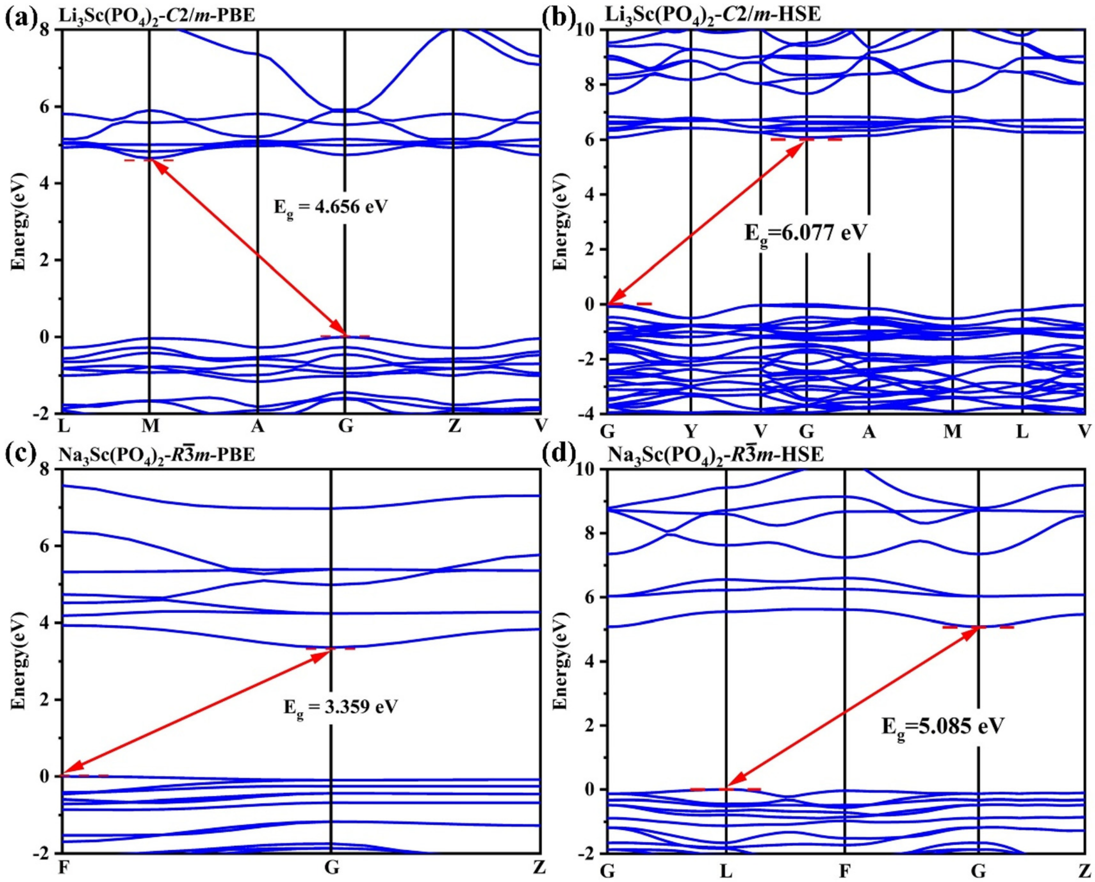

Fig. 5 The GGA–PBE band structures of $Li_3Sc(PO_4)_2$ (a) and $Na_3Sc(PO_4)_2$ (c), and the HSE06 band structures of $Li_3Sc(PO_4)_2$ (b) and $Na_3Sc(PO_4)_2$ (d).

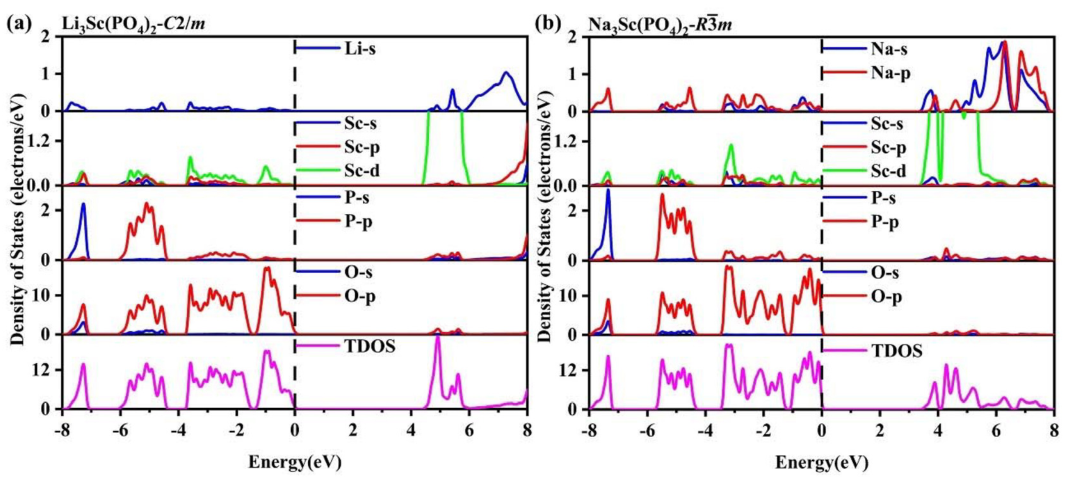

Fig. 6 The PDOS for $A_3Sc(PO_4)_2$ (A = Li, Na): (a) $Li_3Sc(PO_4)_2$ and (b) $Na_3Sc(PO_4)_2$.

group $R\bar{3}m$ and is a uniaxial crystal. The calculated refractive indices are 1.846(n_o) and 1.741(n_e)@532 nm, and 1.741(n_o) and 1.674(n_e)@1064 nm, respectively, distributed according to the rule $n_o > n_e$. Based on the definition of birefringence, the calculated birefringence values are 0.067@532 nm and 0.058@1064 nm. Compared with compounds such as $LiCs_2PO_4$ (E_g = 7.12 eV; Δn(cal) = 0.01@1064 nm),[11] $LiRb_2PO_4$ (E_g = 7.29 eV; Δn = 0.009@1064 nm),[12] $(H_3O)Ca_2Zn_{3.5}(PO_4)_4$ (E_g = 5.69 eV; Δn = 0.002@1064 nm),[18] BPO_4 (E_g = 9.25 eV; Δn = 0.007@1064 nm),[65] and $Ba_3(ZnB_5O_{10})PO_4$ (E_g = 6.89 eV; Δn =

Table 1 The refractive index and birefringence of $A_3Sc(PO_4)_2$ (A = Li, Na)

Compound	Space group	Refractive index			Birefringence
		n_x	n_y	n_z	Δn
$Li_3Sc(PO_4)_2$	$C2/m$	1.772 1.807	1.764 1.801	1.726 1.755	0.046@1064 nm 0.052@532 nm
		n_o	n_e		Δn
$Na_3Sc(PO_4)_2$	$R\bar{3}m$	1.715 1.741	1.657 1.674		0.058@1064 nm 0.067@532 nm

0.033@1064 nm),[66] which also exhibit large bandgaps, the strategy of introducing rare-earth cations as predicted in this paper is thought to be a good strategy as it can maintain a large bandgap and enhanced birefringence.

To further investigate the origin of the large birefringence in $A_3Sc(PO_4)_2$ (A = Li, Na), this study employed the RSAC method[56] to analyze the contributions of each group to the material's birefringence. The results are presented in Table 2. According to the combination of cation and anion groups, $A_3Sc(PO_4)_2$ (A = Li, Na) is composed of Li(Na)O_6 groups, ScO_6 groups, and PO_4 groups. According to the data listed in Table 2, we can observe the following results: (1) the alkali metal cation group (LiO_6 and NaO_6 polyhedra) contributes less to the birefringence of the title compound, with the LiO_6 contribution to birefringence being only 22% (0.023@1064 nm), and the NaO_6 contribution to birefringence being 20%. (2) The rare-earth cation group (ScO_6 octahedra) is the main contributor to the material's birefringence. In $Li_3Sc(PO_4)_2$, the ScO_6 group contributes 54% to the birefringence (0.055@1064 nm, comparable to the birefringence of the $Li_3Sc(PO_4)_2$ crystal), and in $Na_3Sc(PO_4)_2$, the ScO_6 group contributes 60% to the birefringence (0.100@1064 nm). (3) The influence of the anionic group (PO_4 tetrahedra) on the birefringence of the material cannot be ignored, being 24% in $Li_3Sc(PO_4)_2$ (0.024@1064 nm) and 20% in $Na_3Sc(PO_4)_2$ (0.033@1064 nm). Additionally, Tables S2 and S3† record the calculated Born effective charges of $A_3Sc(PO_4)_2$ (A = Li, Na), which further confirms the contribution of the functional modules, the ScO_6 group and the PO_4 group, to the birefringence. It is well known that the electronic structure and arrangement for functional modules are crucial factors influencing the birefringence of materials. In terms of crystal structure, this study found that the PO_4 tetrahedra in $A_3Sc(PO_4)_2$ (A = Li, Na) exhibit a zipper-like arrangement, which has been confirmed to effectively enhance the birefringence of phosphates. In terms of elec-

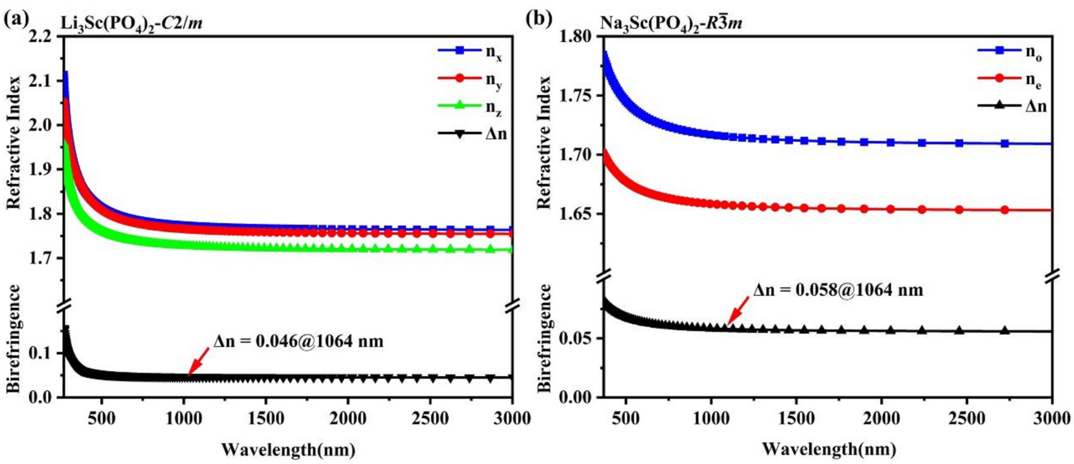

Fig. 7 Refractive index and birefringence of $A_3Sc(PO_4)_2$ (A = Li, Na): (a) $Li_3Sc(PO_4)_2$ and (b) $Na_3Sc(PO_4)_2$.

Table 2 Refractive index and birefringence of groups in $A_3Sc(PO_4)_2$ (A = Li, Na)

Compound	Space group	Group	Refractive index			Birefringence
			n_x	n_y	n_z	Δn (@1064 nm)
$Li_3Sc(PO_4)_2$	$C2/m$	LiO_6 ScO_6 PO_4	1.512 1.501 1.649	1.509 1.491 1.648	1.489 1.446 1.625	0.023 0.055 0.024
			n_o	n_e		Δn (@1064 nm)
$Na_3Sc(PO_4)_2$	$R\bar{3}m$	NaO_6 ScO_6 PO_4	1.541 1.517 1.619	1.406 1.417 1.586		0.035 0.100 0.033

tronic structure, our analysis through PDOS has revealed that the presence of Sc–O bonds near the Fermi level is a determining factor for the optical effects of $A_3Sc(PO_4)_2$ (A = Li, Na).

Conclusion

In summary, this paper successfully screened two new types of rare earth phosphate compounds, $A_3Sc(PO_4)_2$ (A = Li, Na), using a structural search method that combines the ABC algorithm with DFT calculations, and their dynamic stability was proven through stability assessments. The crystal structure of $A_3Sc(PO_4)_2$ (A = Li, Na) indicates that under the control of the ScO_6 group, the PO_4 groups exhibit a zipper-like arrangement. Electronic structural studies indicate that $A_3Sc(PO_4)_2$ (A = Li, Na) maintains the advantage of the large bandgap typical of phosphates, with values of 6.077 eV ($Li_3Sc(PO_4)_2$) and 5.085 eV ($Na_3Sc(PO_4)_2$), respectively. PDOS analysis shows that the large bandgap in $A_3Sc(PO_4)_2$ (A = Li, Na) is mainly contributed by the O-p and Sc-d orbitals. Subsequently, the birefringence and its origins in $A_3Sc(PO_4)_2$ (A = Li, Na) were investigated. The results show that the introduction of rare earth cations significantly enhances the birefringence of phosphates, with values of 0.046@1064 nm ($Li_3Sc(PO_4)_2$) and 0.058@1064 nm ($Na_3Sc(PO_4)_2$), respectively. The real-space atomic cutting method analysis further confirms that the ScO_6 octahedra are the main source of the birefringence gain in $A_3Sc(PO_4)_2$ (A = Li, Na). This study predicts that $A_3Sc(PO_4)_2$ (A = Li, Na) exemplifies a good balance between the bandgap and birefringence in rare earth phosphates, further enriching the variety of rare earth phosphates.

Data availability

The data supporting the findings of this study are included in the article and its ESI.†

Conflicts of interest

The authors declare no conflict of interest related to this work.

Acknowledgements

This work has been supported by the National Natural Science Foundation of China (12264047), the Tianshan Talent Training Program of Xinjiang Uygur Autonomous Region of China (2022TSYCJU0004), the Xinjiang Major Science and Technology Project (2021A01001-3), the Natural Science Foundation of Xinjiang Uygur Autonomous Region (2022D01C419), the XJU Innovation Project for Ph.D candidates (XJU2024BS048), the XJU Innovation Project for M.D candidates (XJU2024G074), the XJU Innovation Project for M.D candidates (XJ2024G074), and the XJU Training Program of Innovation for Undergraduates (202310755096).

References

1 Z. Fang, C.-L. Hu, B.-P. Yang and J.-G. Mao, $Ba_3[Al(PO_4)_3]$: rational design of a promising deep-UV transparent SHG crystal with balanced overall performance originating from the condensation of quartz-type $[Al(PO_4)_4]^{9-}$ units, *J. Mater. Chem. C*, 2021, **9**(5), 1550–1554.
2 C. Wu, L. Li, G. Yang, J. Song, B. Yan, M. G. Humphrey, L. Zhang, J. Shao and C. Zhang, Low-temperature-flux syntheses of ultraviolet-transparent borophosphates $Na_4MB_2P_3O_{13}$ (M = Rb, Cs) exhibiting a second-harmonic generation response, *Dalton Trans.*, 2017, **46**(37), 12605–12611.
3 J. Zhou, P. Gong, M. Xia and Q. Wu, Co-substitution design: a new glaserite-type rare-earth phosphate $K_2RbSc(PO_4)_2$ with high structural tolerance, *Dalton Trans.*, 2023, **52**(43), 15807–15814.
4 D. Pugliese, N. G. Boetti, J. Lousteau, E. Ceci-Ginistrelli, E. Bertone, F. Geobaldo and D. Milanese, Concentration quenching in an Er-doped phosphate glass for compact optical lasers and amplifiers, *J. Alloys Compd.*, 2016, **657**, 678–683.
5 F. F. Sene, J. R. Martinelli and L. Gomes, Optical and structural characterization of rare earth doped niobium phosphate glasses, *J. Non-Cryst. Solids*, 2004, **348**, 63–71.
6 J. Liu, A. M. Kaczmarek and R. Van Deun, Advances in tailoring luminescent rare-earth mixed inorganic materials, *Chem. Soc. Rev.*, 2018, **47**(19), 7225–7238.
7 S. S. Das, P. K. Srivastava and N. B. Singh, Fast ion conducting phosphate glasses and glass ceramic composites: Promising materials for solid state batteries, *J. Non-Cryst. Solids*, 2012, **358**(21), 2841–2846.
8 J. Dang, D. Mei, Y. Wu and Z. Lin, A comprehensive survey on nonlinear optical phosphates: Role of multicoordinate groups, *Coord. Chem. Rev.*, 2021, **431**, 213692.
9 B. Zhang, G. Han, Y. Wang, X. Chen, Z. Yang and S. L. Pan, Expanding Frontiers of Ultraviolet Nonlinear Optical Materials with Fluorophosphates, *Chem. Mater.*, 2018, **30**(15), 5397–5403.
10 D. A. V. Kliner, F. Di Teodoro, J. P. Koplow, S. W. Moore and A. V. Smith, Efficient second, third, fourth, and fifth harmonic generation of a Yb-doped fiber amplifier, *Opt. Commun.*, 2002, **210**(3), 393–398.
11 L. Li, Y. Wang, B.-H. Lei, S. Han, Z. Yang, K. R. Poeppelmeier and S. L. Pan, A New Deep-Ultraviolet Transparent Orthophosphate $LiCs_2PO_4$ with Large Second Harmonic Generation Response, *J. Am. Chem. Soc.*, 2016, **138**(29), 9101–9104.
12 L. Li, Y. Wang, B.-H. Lei, S. Han, Z. Yang, H. Li and S. L. Pan, $LiRb_2PO_4$: a new deep-ultraviolet nonlinear optical phosphate with a large SHG response, *J. Mater. Chem. C*, 2017, **5**(2), 269–274.
13 P. Yu, L.-M. Wu, L.-J. Zhou and L. Chen, Deep-Ultraviolet Nonlinear Optical Crystals: $Ba_3P_3O_{10}X$ (X = Cl, Br), *J. Am. Chem. Soc.*, 2014, **136**, 480–487.
14 Y. Lian, J. Wen, F. Wang, T. Sui, J. Huang, X. Sun and X. Jiang, Nonlinear optical characteristics of an ADP crystal

grown in a defined direction, *Opt. Mater. Express*, 2018, **8**(9), 2614–2624.
15 T. Sui, Y. Lian, M. Xu, L. Zhang, Y. Li, X. Zhao and X. Sun, Stability and electronic structure of hydrogen vacancies in ADP: hybrid DFT with vdW correction, *RSC Adv.*, 2018, **8**(13), 6931–6939.
16 G. Han, Q. Liu, Y. Wang, X. Su, Z. Yang and S. L. Pan, Experimental and theoretical studies on the linear and nonlinear optical properties of lead phosphate crystals $LiPbPO_4$, *Phys. Chem. Chem. Phys.*, 2016, **18**(28), 19123–19129.
17 X. D. Leng, M. Hu, Q. Jing, H. M. Duan, H. L. Chen and Z. H. Chen, The electronic structures and optical properties induced by spin-orbit-coupling in $LiPbPO_4$ compound, *J. Phys. D: Appl. Phys.*, 2024, **57**(32), 325303.
18 T.-Y. Chang, C.-L. Hu, D. Yan and J.-G. Mao, $(H_3O)Ca_2Zn_{3.5}(PO_4)_4$ and $Ba_2Cd_3(PO_4)_2(HPO_4)_2$: Syntheses, crystal structures and characterizations of two mixed metal phosphates, *J. Solid State Chem.*, 2017, **251**, 19–25.
19 X. M. He, L. Qi, W. Y. Zhang, R. X. Zhang, X. Y. Dong, J. H. Ma, M. Abudoureheman, Q. Jing and Z. H. Chen, Controlling the Nonlinear Optical Behavior and Structural Transformation with A-Site Cation in α-$AZnPO_4$ (A = Li, K), *Small*, 2023, **19**(18), 2206991.
20 X. H. Dong, L. Huang, C. F. Hu, H. M. Zeng, Z. E. Lin, X. Wang, K. M. Ok and G. H. Zou, $CsSbF_2SO_4$: An Excellent Ultraviolet Nonlinear Optical Sulfate with a $KTiOPO_4$ (KTP)-type Structure, *Angew. Chem., Int. Ed.*, 2019, **58**(20), 6528–6534.
21 Y. L. Deng, L. Huang, X. H. Dong, L. Wang, K. M. Ok, H. M. Zeng, Z. E. Lin and G. H. Zou, $K_2Sb(P_2O_7)F$: Cairo Pentagonal Layer with Bifunctional Genes Reveal Optical Performance, *Angew. Chem., Int. Ed.*, 2020, **59**(47), 21151–21156.
22 Y. Tian, W. Zeng, X. H. Dong, L. Huang, Y. Q. Zhou, H. M. Zeng, Z. E. Lin and G. H. Zou, Enhanced UV Nonlinear Optical Properties in Layered Germanous Phosphites through Functional Group Sequential Construction, *Angew. Chem., Int. Ed.*, 2024, **63**(36), e202409093.
23 X. H. Dong, L. Huang and G. H. Zou, Rational Design and Controlled Synthesis of High-Performance Inorganic Short-Wave UV Nonlinear Optical Materials, *Acc. Chem. Res.*, 2025, **58**(1), 150–162.
24 L. Xiong, J. Chen, J. Lu, C.-Y. Pan and L.-M. Wu, Monofluorophosphates: A New Source of Deep-Ultraviolet Nonlinear Optical Materials, *Chem. Mater.*, 2018, **30**(21), 7823–7830.
25 X. Zhang, L. Kang, P. Gong, Z. Lin and Y. Wu, Nonlinear optical oxythiophosphate approaching the good balance with wide ultraviolet transparency, strong second harmonic effect, and large birefringence, *Angew. Chem., Int. Ed.*, 2021, **60**(12), 6386–6390.
26 Y. Yang, Y. Qiu, P. Gong, L. Kang, G. Song, X. Liu, J. Sun and Z. Lin, Lone–Pair Enhanced Birefringence in an Alkaline–Earth Metal Tin(II) Phosphate $BaSn_2(PO_4)_2$, *Chem. – Eur. J.*, 2019, **25**(22), 5648–5651.
27 B.-L. Wu, C.-L. Hu, F.-F. Mao, R.-L. Tang and J.-G. Mao, Highly polarizable Hg^{2+} induced a strong second harmonic generation signal and large birefringence in $LiHgPO_4$, *J. Am. Chem. Soc.*, 2019, **141**(26), 10188–10192.
28 J. Zhou, P. Gong, M. Xia, A. Ji, L. Zhang, H. Wu and Q. Wu, Atomic Substitution to Tune ScO_6 Distortion in $Ba_2MSc_2(BO_3)_4$ (M = Na, K, Ba) to Acquire a Large Birefringence, *Inorg. Chem.*, 2023, **62**(23), 8931–8939.
29 T. Sun, P. Shan, H. Chen, X. Liu, H. Liu, S. Chen, Y. A. Cao, Y. Kong and J. Xu, Growth and properties of a noncentrosymmetric polyphosphate $CsLa(PO_3)_4$ crystal with deep-ultraviolet transparency, *CrystEngComm*, 2014, **16**(45), 10497–10504.
30 P. Shan, T. Sun, H. Chen, H. Liu, S. Chen, X. Liu, Y. Kong and J. Xu, Crystal growth and optical characteristics of beryllium-free polyphosphate, $KLa(PO_3)_4$, a possible deep-ultraviolet nonlinear optical crystal, *Sci. Rep.*, 2016, **6**(1), 25201.
31 F. Xu, G. Peng, C. Lin, D. Zhao, B. Li, G. Zhang, S. Yang and N. Ye, $Na_3Sc_2(PO_4)_2F_3$: rational design and synthesis of an alkali rare-earth phosphate fluoride as an ultraviolet nonlinear optical crystal with an enlarged birefringence, *J. Mater. Chem. C*, 2020, **8**(14), 4965–4972.
32 M. Wen, H. Wu, H. Yu and X. Wu, The first rare-earth lead phosphates $Pb_3AP_3O_{12}$ (A = Sc, Gd) with remarkable SHG enhancement, *J. Solid State Chem.*, 2020, **286**, 121276.
33 Y. Shen, Y. Yang, S. Zhao, X. Li, Q. Ding, Y. Li, S. Liu, Z. Lin and J. Luo, A Langbeinite-Type Yttrium Phosphate $LiCs_2Y_2(PO_4)_3$, *Inorg. Chem.*, 2018, **57**(21), 13087–13091.
34 G. Wu, M. Fan, C. Jiang, F. Chen, F. Yu, X. Cheng and X. Zhao, Noncentrosymmetric orthophosphate $YM_3(PO_4)_3$ (M= Sr, Ba) crystals: single crystal growth, structure, and properties, *Cryst. Growth Des.*, 2020, **20**(4), 2390–2397.
35 B.-H. Lei, Z. Yang, H. Yu, C. Cao, Z. Li, C. Hu, K. R. Poeppelmeier and S. L. Pan, Module-Guided Design Scheme for Deep-Ultraviolet Nonlinear Optical Materials, *J. Am. Chem. Soc.*, 2018, **140**(34), 10726–10733.
36 N. Tuerhong, H. H. Chen, M. Hu, X. H. Cui, H. M. Duan, Q. Jing and Z. H. Chen, The enhanced bandgap and birefringence of rare-earth phosphates XPO_4 (X = Sc, Y, La, and Lu): a first-principles investigation, *Phys. Chem. Chem. Phys.*, 2024, **26**(21), 15751–15757.
37 Z. Geng, R. Fu, Z. Ma and X. Wu, $A_3Sc(SO_4)_3$ (A= K, Rb, Cs): Three Deep–Ultraviolet Transparent Alkali–Scandium Sulfates with Strong Second–Harmonic Generation Response and High Thermal Stability, *Adv. Opt. Mater.*, 2024, **12**(29), 2401332.
38 D. Karaboga and B. Akay, A comparative study of Artificial Bee Colony algorithm, *Appl. Math. Comput.*, 2009, **214**(1), 108–132.
39 M. C. Payne, M. P. Teter, D. C. Allan, T. A. Arias and A. J. D. Joannopoulos, Iterative minimization techniques for ab initio total-energy calculations: molecular dynamics and conjugate gradients, *Rev. Mod. Phys.*, 1992, **64**(4), 1045.
40 Y. Wang, J. Lv, L. Zhu and Y. Ma, Crystal structure prediction via particle-swarm optimization, *Phys. Rev. B: Condens. Matter Mater. Phys.*, 2010, **82**(9), 094116.
41 Y. Wang, J. Lv, L. Zhu and Y. Ma, CALYPSO: A method for crystal structure prediction, *Comput. Phys. Commun.*, 2012, **183**(10), 2063–2070.

42 G. Kresse and J. Furthmüller, Efficient iterative schemes for ab initio total-energy calculations using a plane-wave basis set, *Phys. Rev. B: Condens. Matter Mater. Phys.*, 1996, **54**(16), 11169–11186.
43 G. Kresse and J. Furthmüller, Efficiency of *ab initio* total energy calculations for metals and semiconductors using a plane-wave basis set, *Comput. Mater. Sci.*, 1996, **6**(1), 15–50.
44 J. L. Nazareth, Conjugate gradient method, *Wiley Interdiscip. Rev.: Comput. Stat.*, 2009, **1**(3), 348–353.
45 D. A. H. Jacobs, A generalization of the conjugate-gradient method to solve complex systems, *IMA J. Numer. Anal.*, 1986, **6**(4), 447–452.
46 G. Kresse and J. Furthmüller, Efficient iterative schemes for ab initio total-energy calculations using a plane-wave basis set, *Phys. Rev. B: Condens. Matter Mater. Phys.*, 1996, **54**(16), 11169.
47 J. P. Perdew, K. Burke and M. Ernzerhof, Generalized gradient approximation made simple, *Phys. Rev. Lett.*, 1996, **77**(18), 3865.
48 D. R. Hamann, M. Schlüter and C. Chiang, Norm-conserving pseudopotentials, *Phys. Rev. Lett.*, 1979, **43**(20), 1494.
49 H. J. Monkhorst and J. D. Pack, Special points for Brillouin-zone integrations, *Phys. Rev. B*, 1976, **13**(12), 5188.
50 S. J. Clark, M. D. Segall, C. J. Pickard, P. J. Hasnip, M. I. J. Probert, K. Refson and M. C. Payne, First principles methods using CASTEP, *Z. Kristallogr. - Cryst. Mater.*, 2005, **220**(5–6), 567–570.
51 W. Jia, J. Fu, Z. Cao, L. Wang, X. Chi, W. Gao and L.-W. Wang, Fast plane wave density functional theory molecular dynamics calculations on multi-GPU machines, *J. Comput. Phys.*, 2013, **251**, 102–115.
52 W. Jia, Z. Cao, L. Wang, J. Fu, X. Chi, W. Gao and L.-W. Wang, The analysis of a plane wave pseudopotential density functional theory code on a GPU machine, *Comput. Phys. Commun.*, 2013, **184**(1), 9–18.
53 M. K. Y. Chan and G. Ceder, Efficient band gap prediction for solids, *Phys. Rev. Lett.*, 2010, **105**(19), 196403.
54 J. Paier, M. Marsman, K. Hummer, G. Kresse, I. C. Gerber and J. G. Ángyán, Screened hybrid density functionals applied to solids, *J. Chem. Phys.*, 2006, **124**(15), 154709.
55 A. V. Krukau, O. A. Vydrov, A. F. Izmaylov and G. E. Scuseria, Influence of the exchange screening parameter on the performance of screened hybrid functionals, *J. Chem. Phys.*, 2006, **125**(22), 224106.
56 J. Lin, M.-H. Lee, Z.-P. Liu, C. Chen and C. J. Pickard, Mechanism for linear and nonlinear optical effects in β-BaB_2O_4 crystals, *Phys. Rev. B: Condens. Matter Mater. Phys.*, 1999, **60**(19), 13380–13389.
57 W. H. Baur, The geometry of polyhedral distortions. Predictive relationships for the phosphate group, *Acta Crystallogr., Sect. B:Struct. Sci.*, 1974, **30**, 1195–1215.
58 K. Momma and F. Izumi, VESTA3 for three-dimensional visualization of crystal, volumetric and morphology data, *J. Appl. Crystallogr.*, 2011, **44**, 1272–1276.
59 I. Carrasco, K. Barrtosiewicz, F. Piccinelli, M. Nikl and M. Bettinelli, Structural effects and 5d→4f emission transition shifts induced by Y co-doping in Pr-doped $K_3Lu_{1-x}Y_x(PO_4)_2$, *J. Lumin.*, 2017, **189**, 113–119.
60 J. M. Farmer, L. A. Boatner, B. C. Chakoumakos and C. J. Rawn, Structural and crystal chemical properties of alkali rare-earth double phosphates, *J. Alloys Compd.*, 2016, **655**(15), 253–265.
61 J. M. Farmer, L. A. Boatner, B. C. Chakoumakos, C. J. Rawn, D. Mandrus, R. Y. Jin and J. C. Bryan, Polymorphism, phase transitions, and thermal expansion of $K_3Lu(PO_4)_2$, *J. Alloys Compd.*, 2014, **588**(5), 182–189.
62 J. Wang, H. Zhang, M. Jiang, M. Nikitina, V. Maltsev and N. Leonyuk, Flux Growth and External Morphology of $KTiOPO_4$ Crystals, *Cryst. Growth Des.*, 2009, **9**(2), 1190–1193.
63 M. Wen, C. Hu, Z. Yang, X. Wu and S. L. Pan, $K_2TeP_2O_8$: a new telluro-phosphate with a pentagonal Te-P-O layer structure, *Dalton Trans.*, 2018, **47**(28), 9453–9458.
64 Y. Zhou, L. Cao, C. Lin, M. Luo, T. Yan, N. Ye and W. Cheng, $AMgPO_4{\cdot}6H_2O$ (A = Rb, Cs): strong SHG responses originated from orderly PO_4 groups, *J. Mater. Chem. C*, 2016, **4**(39), 9219–9226.
65 X. Zhang, L. Wang, S. Zhang, G. Wang, S. Zhao, Y. Zhu, Y. Wu and C. Chen, Optical properties of the vacuum-ultraviolet nonlinear optical crystal - BPO_4, *J. Opt. Soc. Am. B*, 2011, **28**(9), 2236–2239.
66 H. W. Yu, W. G. Zhang, J. S. Young, J. M. Rondinelli and P. S. Halasyamani, Design and Synthesis of the Beryllium-Free Deep-Ultraviolet Nonlinear Optical Material $Ba_3(ZnB_5O_{10})PO_4$, *Adv. Mater.*, 2015, **27**(45), 7380–7385.
67 Y. H. Hu, X. Xu, R. X. Wang, J. Y. Han, S. S. Zhang, S. H. Zhan, J. Y. Guo, L. M. Wu and L. Chen, $[Sn_3OF]PO_4$ vs $[Sn_3F_3]PO_4$: Enhancing Birefringence through Breaking R3 Symmetry and Realigning Lone Pairs, *Inorg. Chem. Front.*, 2024, **11**, 5648–5656.
68 L. H. Deng, R. Zhang, N. J. Zhang, W. L. Xie, C. Y. Bai, Z. H. Yang, X. L. Hou, S. J. Han and S. L. Pan, Stereochemically Active Tin(II)-Induced Enhancement of Birefringence in $SnIISnIV(PO_4)_2$ and $SrSn(PO_4)PO_2(OH)_2$, *Chem. – Eur. J.*, 2023, **29**, e202300743.
69 R. T. Song, Z. Q. Yang, H. Z. Zhang, X. Q. Tang, Y. X. Liu and J. Zhu, Highly thermally stable and tunable luminescence in microwave-assisted synthesized $Na_3Ca_4(TeO_3)(PO_4)_3$:Dy^{3+}, Eu^{3+} for ultra-high color rendering white light-emitting diodes, *Ceram. Int.*, 2023, **49**(13), 22323–22331.
70 M. Y. Ji, C. L. Hu, Z. Fang, Y. Chen and J. G. Mao, Tin(II)-Induced Large Birefringence Enhancement in Metal Phosphates, *Inorg. Chem.*, 2021, **60**, 15744–15750.
71 C. Wu, X. X. Jiang, Z. J. Wang, H. Y. Sha, Z. S. Lin, Z. P. Huang, X. F. Long, M. G. Humphrey and C. Zhang, UV Solar-Blind-Region Phase-Matchable Optical Nonlinearity and Anisotropy in a π-Conjugated Cation-Containing Phosphate, *Angew. Chem., Int. Ed.*, 2021, **60**(27), 14806–14810.